Joint-LSRTM in practice with the Deimos ocean bottom field data set

Mandy Wong, Biondo Biondi, and Shuki Ronen

ABSTRACT

We apply an adaptation of the least-squares reverse time migration (LSRTM) algorithm to the 3D Deimos ocean bottom field data set from the Gulf of Mexico. A simple data-fitting objective function may not be sufficient when applying LSRTM in practice. Some challenges arise because the recorded field data depart from the theory and assumption of the LSRTM operator. To optimize the inversion with the field data set, we include Laplacian preconditioning, salt-dimming data weighting, extended domain noise filtering, and regularization onto the LSRTM algorithm. Results from the 3D Deimos ocean bottom field dataset show an improvement when using joint LSRTM of primary and mirror signals over conventional imaging.

INTRODUCTION

Depth migration images are often distorted by uneven subsurface illumination from acquisition geometry, complex overburden and band-limited wavefields. To correct for the effects of uneven illumination, the imaging problem can be posed as a linear inverse problem. Depth migration is equivalent to the adjoint of the Born-modelling operator. Instead of using the adjoint operator, we use the pseudo-inverse of the Born-modeling operator to optimally reconstruct the reflectivity. This inversion-based imaging method is also widely known as least-squares migration (LSM) (Lambare et al., 1992; Nemeth et al., 1999; Ronen and Liner, 2000) or linearized wavefield inversion (Clapp, 2005; Valenciano, 2008a).

In addition to least-squares migration, being able to co-image different types of seismic data can often add value to the image. In the case of ocean-bottom data, Wong et al. (2010) showed that using both primary (up-going) and mirror (down-going) signals can improve subsurface illumination. The mirror image has wider illumination. Depending on the offset range and the ocean-bottom depth, primary signal can often illuminate the subsurface at a wider reflection angle (Figure 1). This translates to higher image quality in the region illuminated by the primary. Instead of treating the primary image and the mirror image separately, we can combine the information from the two sets of data coherently by joint least-squares reverse-time migration (LSRTM)

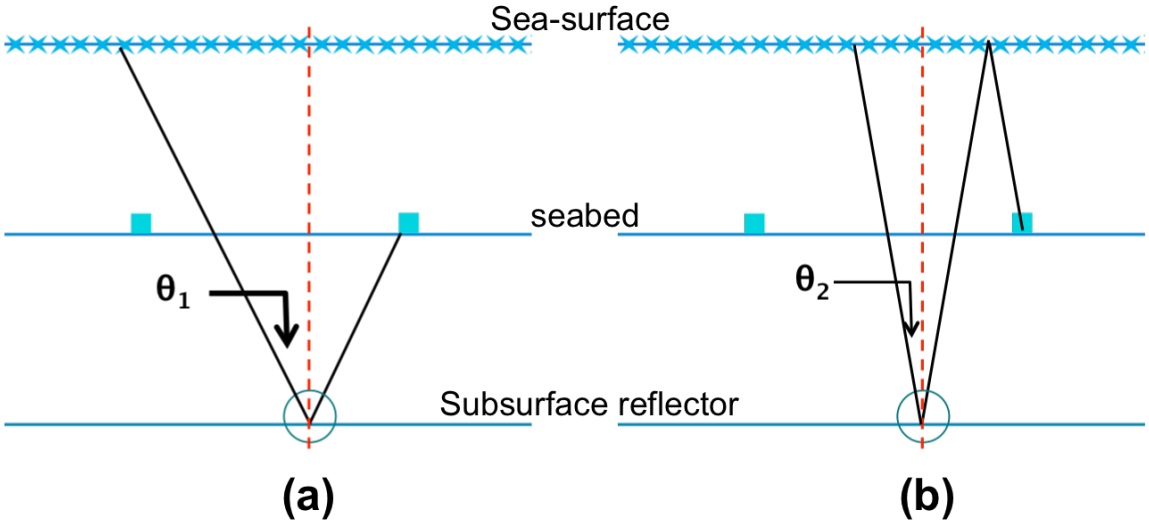

Figure 1: (a) shows the reflection angle (θ_1) by the primary reflection and (b) shows the reflection angle (θ_2) by the mirror reflection at the same sub-surface image location for ocean bottom node acquisition geometry. Given a survey with limited offset, the primary signal can often illuminate the subsurface at a wider reflection angle. [**NR**]

LSM in general can boost up the signal for the true reflector and suppress noise. When applied to a field data set, the quality of the inversion can be compromised by various factors. As a result, adaptation and conditioning of the inversion is needed when applying to the field data set. We will point out a few of the challenges concerning the 3D Deimos ocean bottom data set and show some ways to address these issues. Some of the techniques include Laplacian preconditioning, salt-dimming data weighting (Wong et al., 2010), extended domain noise filtering, and a regularization that impose continuity along the subsurface-angle axis.

In this paper, we will apply joint up-going (primary) and down-going (mirror) least-squares reverse-time migration (LSRTM) on the 3D Deimos ocean bottom node field data set. I will show some of the improvements as compared to conventional imaging.

THEORY

Least-squares reverse-time migration (LSRTM)

In reverse-time migration (RTM), the migration image is a linear operator applied to the recorded data,

$$\begin{aligned} m_{mig}(\mathbf{x}) &= \sum_{\mathbf{x_r},\mathbf{x_s},\omega} U_s^*(\mathbf{x_s},\mathbf{x},\omega) G^*(\mathbf{x},\mathbf{x_r}) d(\mathbf{x_r},\mathbf{x_s},\omega), \\ &= \mathbf{L'd}, \end{aligned} \tag{1}$$

where ω is frequency and $m(\mathbf{x})$ represents reflectivity at the image point $\mathbf{x}$. Additionally, $U_s(\mathbf{x_r}, \mathbf{x}, \omega) = \omega^2 f_s(\omega) G(\mathbf{x_r}, \mathbf{x})$ is the source-side or incident wavefield. $G(\mathbf{x_1}, \mathbf{x_2})$ is the Green function that solves the two-way acoustic constant density equation. Often time, deconvolution is performed on the input data $d(\mathbf{x_r}, \mathbf{x_s}, \omega)$ and an appropriate waveform $f_s(\omega)$ is used to generate the source-side wavefield. Note that the ω dependence in G is suppressed. The RTM operator can be abbreviated into the operator form $\mathbf{L}'$ acting on the data $\mathbf{d}$. In practice, the Green function is calculated using finite-difference time domain technique and the multiplication in frequency domain is replaced by a zero-lag cross-correlation in the time domain.

To obtain a better reflectivity image, we can go beyond migration by formulating the imaging problem as a least-squares inversion problem. The solution $m_{inv}(\mathbf{x})$ is obtained by minimizing the objective function $S(\mathbf{m})$, which is defined as the least-squares difference between the forwarded modeled data d_{mod} and the observed data d_{obs}.

$$S(\mathbf{m}) = \|\mathbf{d_{mod}} - \mathbf{d_{obs}}\|^2 = \|(\mathbf{Lm} + \mathbf{d_o}) - \mathbf{d_{obs}}\|^2 \tag{2}$$

The modeled data $\mathbf{d_{mod}}$ can be broken down into two components: the linearly modeled data $\mathbf{Lm}$ and the background data $\mathbf{d_o}$. The background data is the full wave-equation modeling of the data using the (background) migration velocity model. $\mathbf{d_o}$ does not get updated, and remains the same over all iterations in the least-squares migration algorithm.

In LSRTM, the linear forward modeled data is defined to be the Born approximation of the linearized acoustic wave equation,

$$\begin{aligned} d_{mod}(\mathbf{x_r}, \mathbf{x_s}, \omega) &= \sum_{\mathbf{x}} U_s(\mathbf{x_s}, \mathbf{x}, \omega) m(\mathbf{x}) G(\mathbf{x}, \mathbf{x_r}), \\ \mathbf{d_{mod}} &= \mathbf{Lm}, \end{aligned} \tag{3}$$

It is important to point out that the forward modeling operator $\mathbf{L}$ is the adjoint of the reverse-time migration operator $\mathbf{L}'$.

Joint LSRTM of up/down-going P wave

Joint inversion of up- and down-going signals for ocean-bottom data can potentially be a better imaging technique than migrating either signal alone, because it combines information from both sets of signals. Ocean bottom data are first separated into acoustic up- and down-going components above the seafloor. The decomposed signals are then inverted to yield one optimally combined reflectivity image. The objective function for such an inversion is:

$$S(\mathbf{m}) = \|(\mathbf{L}_\uparrow \mathbf{m} + \mathbf{d}_\mathbf{o}^\uparrow) - \mathbf{d}_\mathbf{obs}^\uparrow\|^2 + \|(\mathbf{L}_\downarrow \mathbf{m} + \mathbf{d}_\mathbf{o}^\downarrow) - \mathbf{d}_\mathbf{obs}^\downarrow\|^2 \tag{4}$$

where $\mathbf{L}_\uparrow$ and $\mathbf{L}_\downarrow$ are modeling operators that linearly model the up- and down-going data. Two modified grids are used to forward model the lowest order of up- and

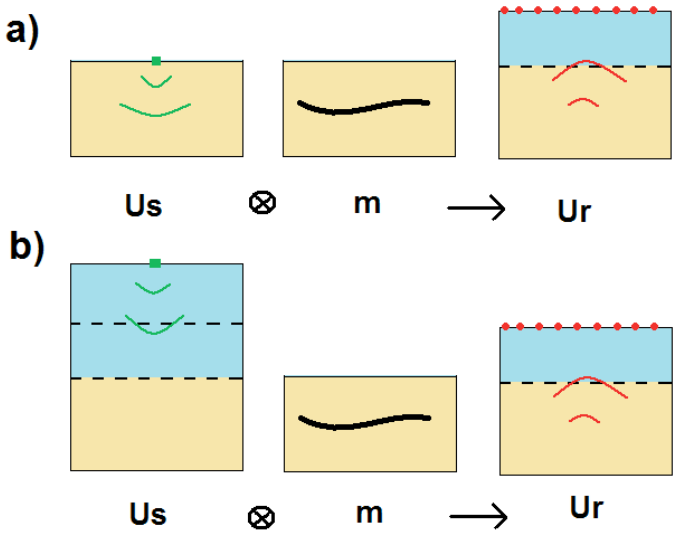

Figure 2: Forward modeling of (a) primary-only and (b) mirror-only data. The algorithm involves cross-correlating the source wavefield (U_s) with the reflectivity model (m) to generate the receiver wavefield (U_r). Reciprocity is used here where the data, in common-receiver domain, is injected at the source location while the source wavelet is injected at the receiver location. Cross-correlation is done only with grid points below the seabed. [**NR**]

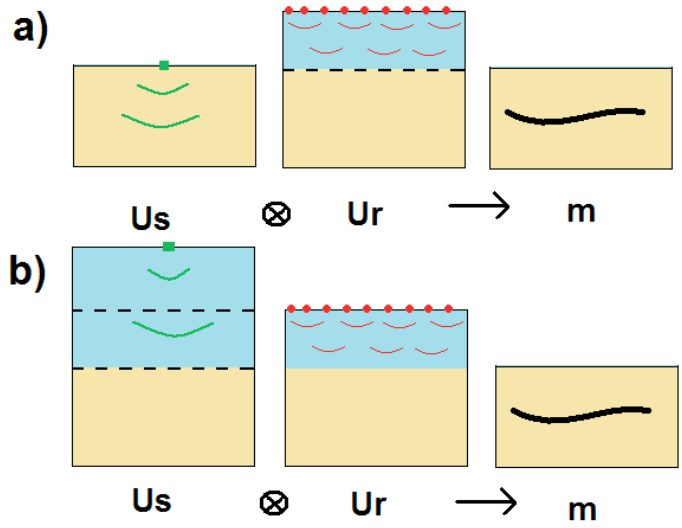

Figure 3: RTM of (a) primary-only and (b) mirror-only data. The algorithm involves cross-correlating the source wave field (U_s) with the receiver wave field (U_r) to generate the reflectivity model (m). Cross-correlation is done only with grid points below the seabed. [**NR**]

down-going signals, namely the primary and the mirror reflection. The formulation of the modeling operator is summarized in Figure 2 and 3

Although LSM in general can boost up the signal for true reflectors and suppress noise, the quality of the inversion may compromised when applied to a field data set. As a result, adaptation and conditioning of the inversion is needed when applying to the field data set. We will point out a few of the challenges and show some ways to address those issues.

Laplacian Preconditioning

It has been observed that using the conventional cross-correlation imaging condition produces strong low-frequency migration artifacts in reverse-time migration. These artifacts result from the forward-scattered energy off sharp contrast in the velocity model. In LSRTM, a successive sequence of adjoint and modeling operations is required to iteratively change the initial solution into the inverted one. As a result, when the adjoint operation is used in LSRTM, the forward-scattering artifacts also exist in the gradient. Such artifacts hamper the convergence because unwanted energy is introduced into the gradient at every iteration. One way to suppress these artifacts is to apply a Laplacian filter to the stacked RTM image. Zhang and Sun (2009) have showed that applying the Laplacian filter (along with a $1/\omega^2$ filter onto the data) is equivalent to applying a $cos^2\theta$ weight to the angle gather. This cosine factor down-weights contributions from large angles and effectively suppresses the forward-scattered artifacts when $\theta = 90^o$. A straightforward incorporation of this idea in LSRTM is to use the Laplacian filter as a preconditioner in the inversion. This can be done by doing a simple change of variable,

$$\mathbf{p} = \mathbf{Am}, \tag{5}$$

where $\mathbf{A}$ represents the Laplacian operator and $\mathbf{p}$ is the preconditioned variable. Note that the Laplacian operation is self-adjoint. The objective function in terms of the preconditioned variable $\mathbf{p}$ then becomes:

$$S(\mathbf{p}) = \|(\mathbf{L}_\uparrow \mathbf{Ap} + \mathbf{d}_\mathbf{o}^\uparrow) - \mathbf{d}_\mathbf{obs}^\uparrow\|^2 + \|(\mathbf{L}_\downarrow \mathbf{Ap} + \mathbf{d}_\mathbf{o}^\downarrow) - \mathbf{d}_\mathbf{obs}^\downarrow\|^2 \tag{6}$$

After inverting for $\mathbf{p}_{inv}$, the inverted model is then recovered by applying the inverse of the Laplacian operator,

$$\mathbf{m}_{inv} = \mathbf{A^{-1}} \mathbf{p}_{inv}. \tag{7}$$

The inverse of the Laplacian operator is singular. In practice, we applied a pseudo inverse in the wavenumber domain by multiplying a $\frac{1}{k_z^2+\epsilon}$ filter with a small ϵ constant.

Salt Dimming

The objective function in equation 2 requires the background data term $\mathbf{d_o}$ to be subtracted from the observed data. Essentially, $\mathbf{d_o}$ is the forward modeling using the migration velocity model. In most cases when the velocity is smoothly varying, this term is negligible and we can just ignore it in the inversion. When the velocity field has a sharp contrast, this term is non-trivial. However, subtracting the background data term is actually a difficult task. The theory that generates the background data is just an approximation to the complex Earth mechanism that generates the observed data. This makes following equation 2 impractical. Salt-dimming (Wong, 2013) is introduced as a way to work around this problem.

Salt-dimming aims to down-weight the salt reflection energy in the data space so that the inversion can minimize other regions in the model. This corresponds to the following objective function:

$$S(\mathbf{m}) = \|\mathbf{W}_s(\mathbf{L}m - d^{obs})\|^2,$$

where $\mathbf{W_s}$ is the data weighting function that down-weights the salt reflection energy. This can be done by forward-modeling the salt reflection using the migration velocity. The next step is to calculate an envelope around the salt energy. The data weighting function can then be defined by assigning a small value to the salt reflection envelope. The objective function with preconditioning and salt-dimming then becomes:

$$S(\mathbf{p}) = \|\mathbf{W}_s^{\uparrow}(\mathbf{L}_{\uparrow}\mathbf{A}\mathbf{p} - \mathbf{d}_{\mathbf{obs}}^{\uparrow})\|^2 + \|\mathbf{W}_s^{\downarrow}(\mathbf{L}_{\downarrow}\mathbf{A}\mathbf{p} - \mathbf{d}_{\mathbf{obs}}^{\downarrow})\|^2. \tag{8}$$

Figure 4a shows the forward modeling of one common-receiver gather in the synthetic Sigbees model. The salt reflection is then used to derive an envelope region to be down-weighted. The resulting weighting function is shown in Figure 4b. As shown in Figure 4b the down-weighted region (blue) corresponds mostly to the salt reflector.

Noise removal in the extended domain

Unwanted noise sometimes appears in the migrated images. For example, when internal multiples are not properly removed, migrating that energy with an operator that only accounts for the kinematics of the primary would result in crosstalk noise in the image. In ocean bottom data sets, imperfect PZ summation or up-down decomposition can also result in artifacts in the migrated image. Another source of noise comes from our attempt to invert elastic data with acoustic waves thoery. For example, converted wave are in the data but are not accounted for in the modeling and migration operator. Ideally, we want all unaccounted events to be removed in the field data before migration or least-squares migration. LSRTM can be hampered when noise energy remains in the data.

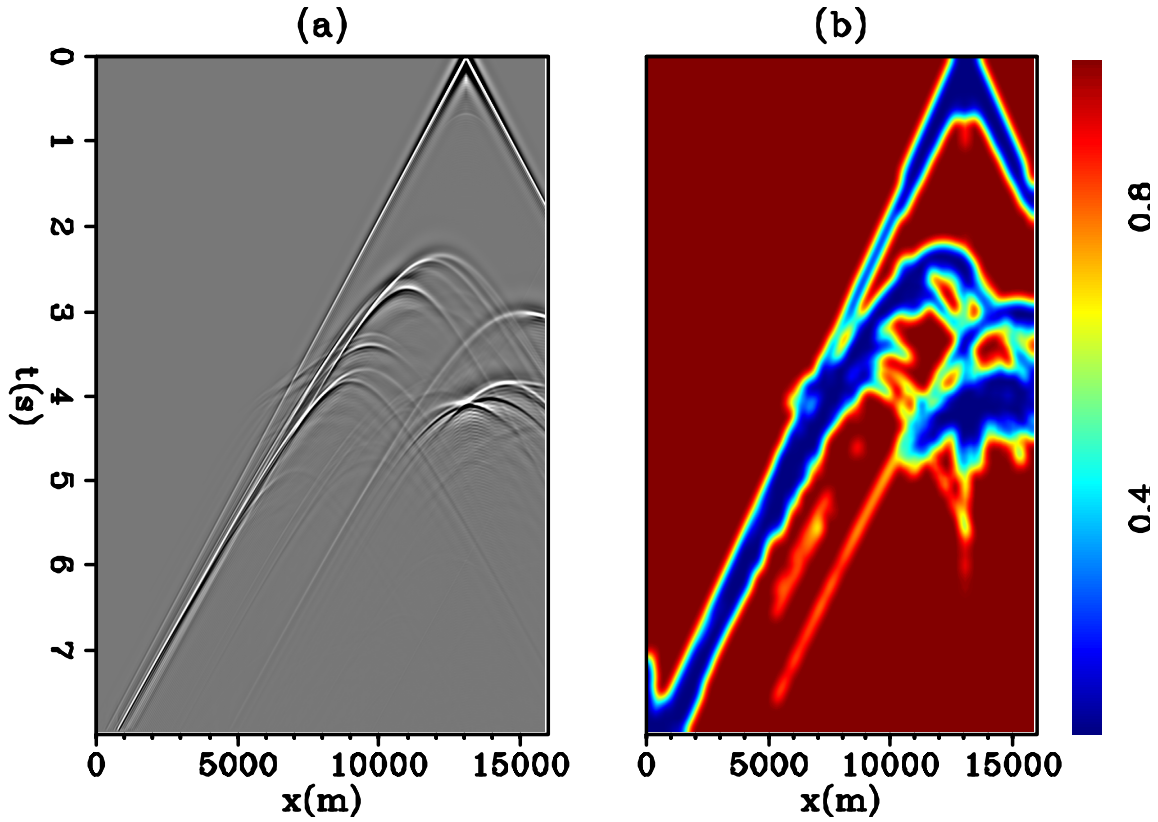

Figure 4: (a) Background data created by forward modeling with the migration velocity and (b) salt-dimming weight (W_s) generated with the background data. [**CR**]

To make the algorithm more robust, we utilize the subsurface offset domain to filter some of the unwanted noise in the image space. Figure 5 shows an offset-domain common image gather (ODCIG) for one of the ocean bottom node. The front face corresponds to the image at zero subsurface offset and the side face corresponds to the depth-offset panel at a horizontal location. Notice how the energy in the depth-offset panel is tilted based on its relative position from the source. In Figure 5a, the horizontal position is less than x_{shot}. In this case, the prominent energy in the depth-offset panel is tilted with a negative slope. Similarly, in Figure 5c, the horizontal position is greater than x_{shot}. In this case, the prominent energy in the depth-offset panel is tilted with a positive slope. When we examine the depth-offset gather at a horizontal position that is close to the source, as shown in Figure 5b, the prominent energy has near zero slope.

This characteristic can be used to discriminate some of the noise in the image space. A filter was designed and applied for each ocean bottom node's ODCIG before summing together. For each ODCIG, we apply the Fourier transform of each depth-offset slice into the $k_z - k_{\text{hx}}$ wavenumber space. In the wavenumber space, a dominant dip energy range can be selected as signal while the other energy can be filtered out as noise. The dip-range can be estimated based on the horizontal x position of the $k_z - k_{\text{hx}}$ slice relative to the shot position x_{shot}. We used a large dip range (60 degrees) to avoid filtering out true reflector signal. Seismic waves are often severely distorted and bent by the salt, which could result in true signal forming at various dip in the $z - h$ panel. We have used a different set of filtering criteria for the region beneath the salt so that the true signal will not be filtered out.

Physically, filtering the dips in the depth-offset domain is equivalent to filtering in angle domain. Recall the relationship that links the dips in the depth-offset domain to the aperture angle (γ):

$$\frac{k_{\text{hx}}}{k_z} = -\tan\gamma. \tag{9}$$

We are making the assumption that, based on the horizontal distance between the image point with x_{shot}, signal can only be formed with a particular aperture angle range.

Although equation 9 is only true in 2D, an equivalent expression in 3D that include the reflector's tilt exist. For this praticular dataset, the dipping along the crossline direction is minimal. An equivalent filtering procedure involving k_{hy} can be applied in 3D when the crossline dip is signicant.

Figure 6 shows the result of extended domain filtering on a single prestack subsurface offset image gather. Most of the noise is removed above the salt reflection at $z = 4000m$. Figure 7 shows an enlarged section of Figure 6. The original prestack RTM image (Figure 7a) is decomposed into the signal part (Figure 7b) and the noise part (Figure 7c) by using extended-domain noise filtering. In our LSRTM algorithm, the extended-domain filtering is used to remove some of the noise in the gradient. A similar approach was used by Valenciano (2008b). Instead of filtering in the $k_z - k_{\text{hx}}$

space, Valenciano (2008b) filter out salt-related internal multiples in the $kx - k_{\text{hx}}$ wavenumber space.

Regularization that penalizes discontinuity along the reflection angle

We used the regularization term inClapp (2005) to penalize discontinuity along the subsurface reflection angle axis. This can be done by multiplying the factor h_x onto the ODCIG. We represent the regularization operator with $\mathbf{D}$ as shown,

$$\epsilon \mathbf{D}\mathbf{p} = \epsilon h_x p(x, y, z, h_x). \tag{10}$$

In LSRTM, it can be added as a regularization term to help focus the subsurface-offset energy to zero-offset. The value of ϵ is chosen such that the model fitting term is roughly about 5 percents of the data fitting term at the first iteration. As the data-fitting residual decreases over iterations, the relative contribution from the regularization increases. The final objective function looks like:

$$S(\mathbf{p}) = \|\mathbf{W}_s^{\uparrow}(\mathbf{L}_{\uparrow}\mathbf{A}\mathbf{p} - \mathbf{d}_{\mathbf{obs}}^{\uparrow})\|^2 + \|\mathbf{W}_s^{\downarrow}(\mathbf{L}_{\downarrow}\mathbf{A}\mathbf{p} - \mathbf{d}_{\mathbf{obs}}^{\downarrow})\|^2 + \|\epsilon\mathbf{D}\mathbf{p}\|^2, \tag{11}$$

where $\mathbf{D}$ represents the DSO operator. Notice that the DSO is acting on the preconditioned variable $\mathbf{p}$ instead of the model $\mathbf{m}$. By dampening on the preconditioned variable $\mathbf{p}$, the regularization term effectively penalizes large values in $\|\epsilon\mathbf{D}\mathbf{A}^{-\mathbf{1}}\mathbf{m}\|^2$. This effectively penalizes discontinuity at smaller reflection angle more than at larger reflection angle.

RESULTS

Deimos 3D ocean bottom node dataset

The Deimos data set was recorded in an area approximately south-east of New Orleans in the Gulf of Mexico. The field was discovered in 2002, with first oil production in 2007 (Burch et al., 2010; Smit et al., 2008; Stopin et al., 2008). In 2007, Shell Exploration and Production Company and their partner BP Americas commissioned Fairfield Industries to conduct a 3D ocean bottom node survey over the Deimos field in the Mississippi Canyon protration area. The survey was acquired with a 400 x 400 m grid of 807 ocean bottom nodes with a 50 x 50 m shot grid. Before the 3D survey began, a pilot mini-survey of 16 ocean bottom nodes were deployed on a single 2D line at their normal 3D grid locations (Hays et al., 2008). A swath of seven dual-source sail lines nearest the node line were shot. This gives fourteen source lines on the nominal 50x50 m grid for about 3300 shots. Figure 8 shows the location of the sources and the receivers.

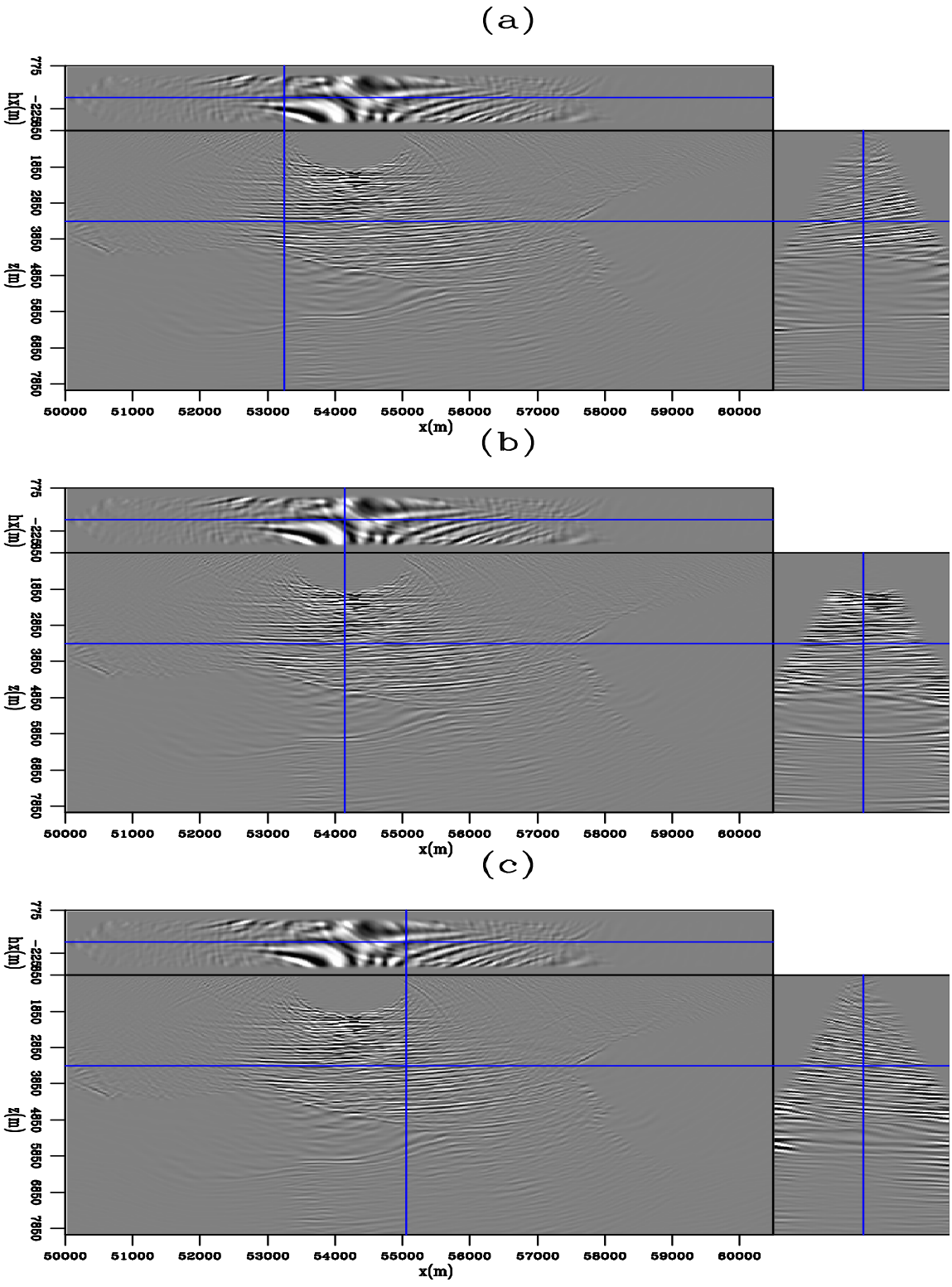

Figure 5: A prestack subsurface offset image gather with a single node located at x=54350 m and y=34800 m. The image cube is displayed at a constant crossline slice of y=54350 m and with the horizontal slice displayed (a) to the left, (b) at the center, and (c) to the right of the horizontal shot location. Notice how the energy in the depth-offset panel is tilted based on its relative position from the source. [**CR**]

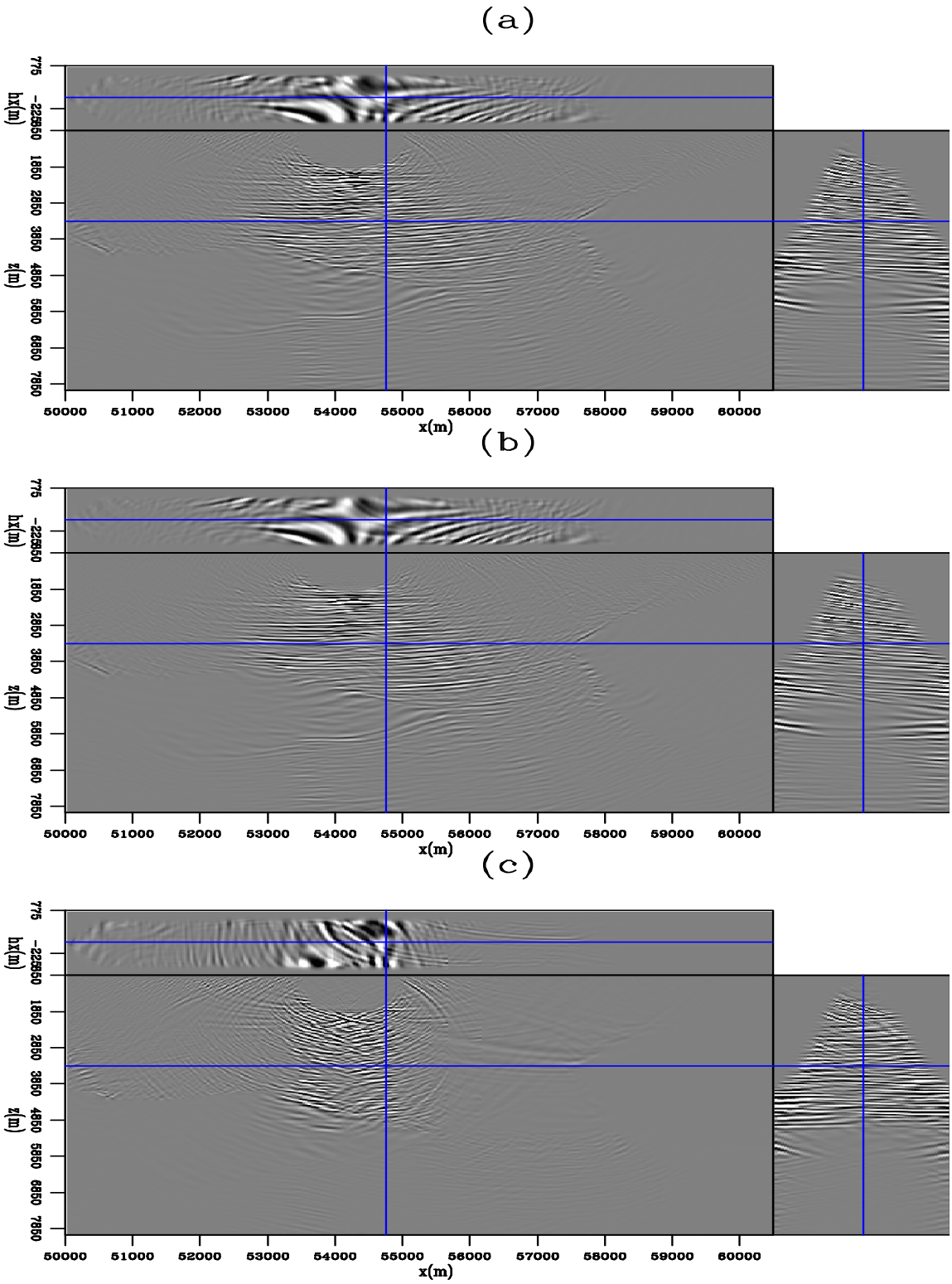

Figure 6: The same prestack subsurface offset image gather from Figure 5 with the horizontal slice displayed at x=54750 m (a) before filtering (b) after filtering, and (c) filtered noise. The sum of (b) and (c) should be the same as (a). [**CR**]

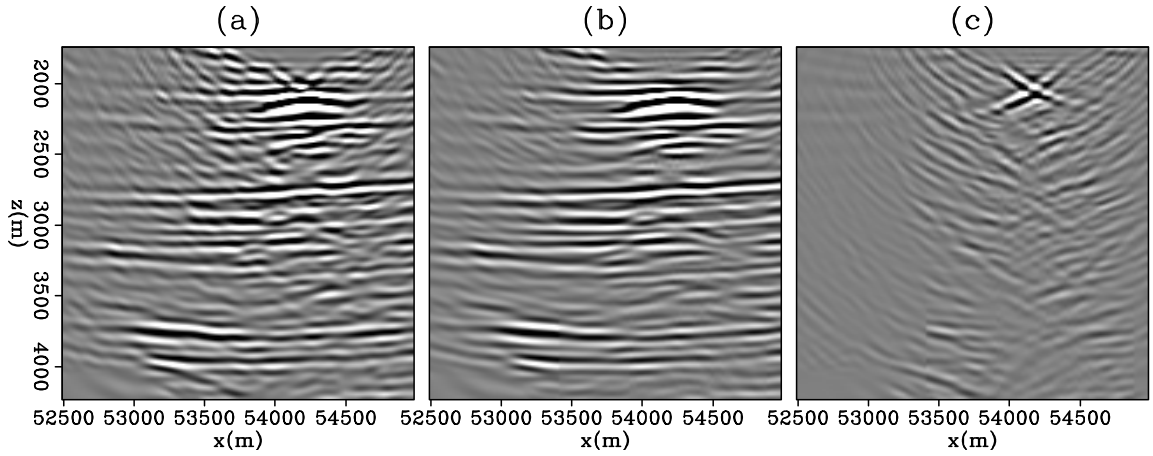

Figure 7: An enlarged section of Figure 6 (a) before filtering, (b) after filtering, and (c) filtered noise. The sum of (b) and (c) should be the same as (a). [**CR**]

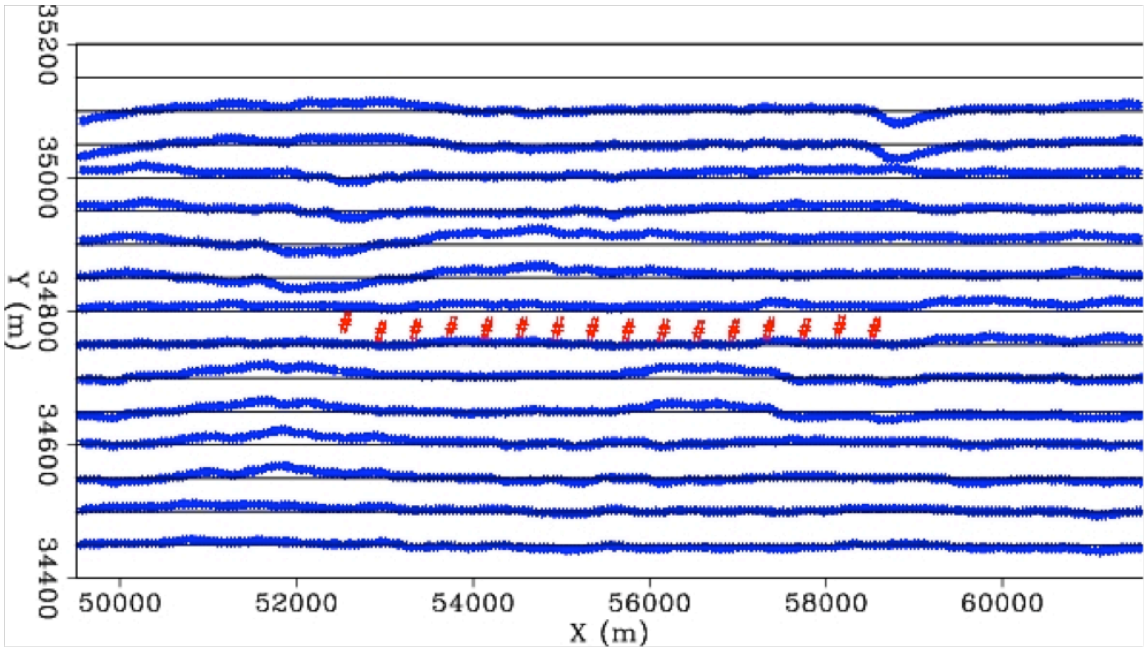

Figure 8: The acquisition geometry for the Deimos ocean bottom data set. The 14 source lines span a 50 x 50 m grid. The 16 ocean bottom node receivers are deployed on a 2D line with an approximate spacing of 400 m. [**NR**]

This is effectively a narrow azimuth survey where the horizontal (in-line) extent is much greater than the vertical (crossline) extent. As a result, inline dipping reflectors should be much better resolved than crossline dipping reflectors. Prior knowledge of this field suggests that there are fewer structural variations along the crossline direction compared to the inline direction. Figure 9 shows the migration velocity model used in this study.

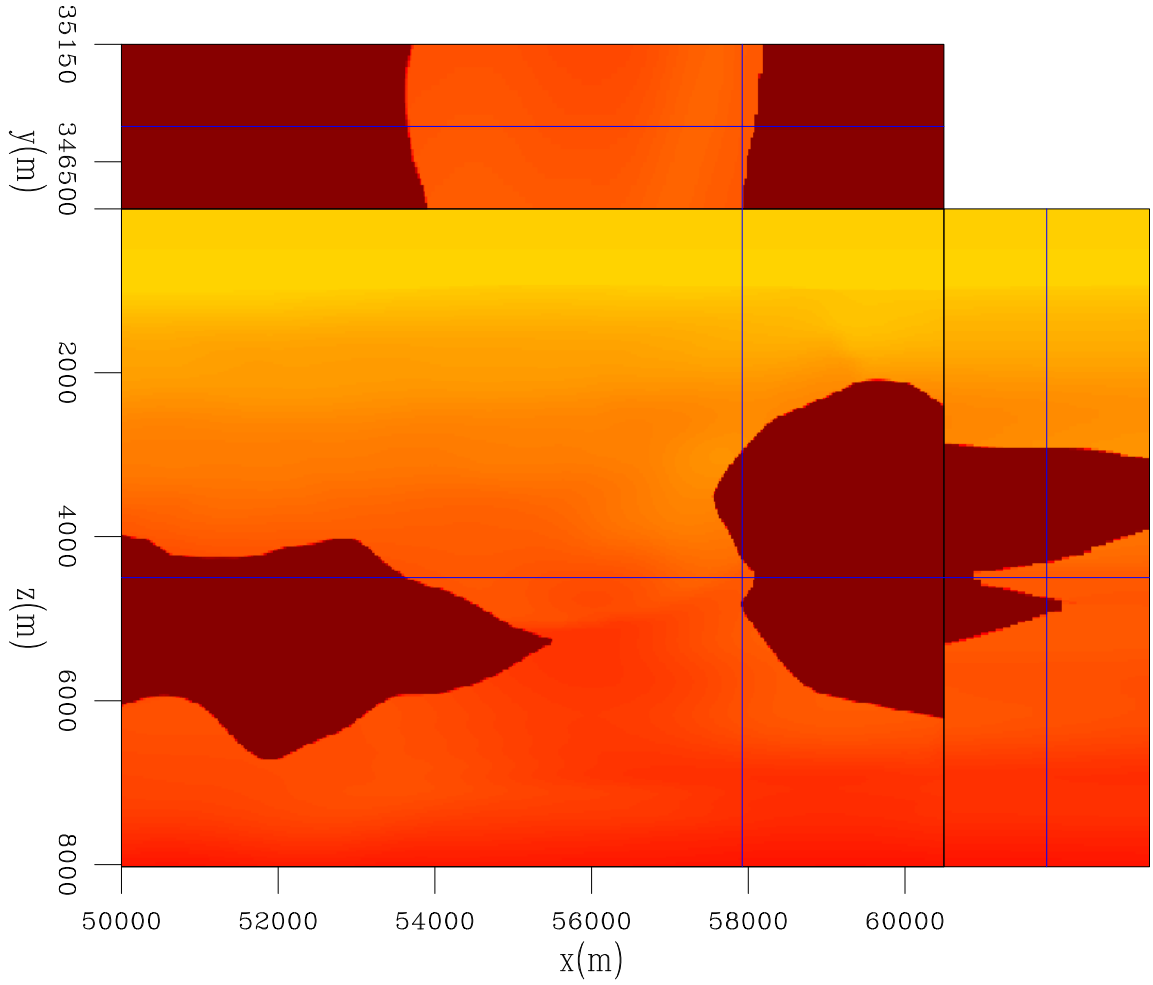

Figure 9: The migration velocity model used for the 16 nodes of the Deimos ocean bottom node survey. [**CR**]

Pre-processing

Shell Exploration and Production Company performed some pre-processing of this ocean bottom node dataset. PZ summation and multiple removal are performed to extract the up- and down-going signal from the dataset. Figure 10 shows the up-going and down-going data after pre-processing.

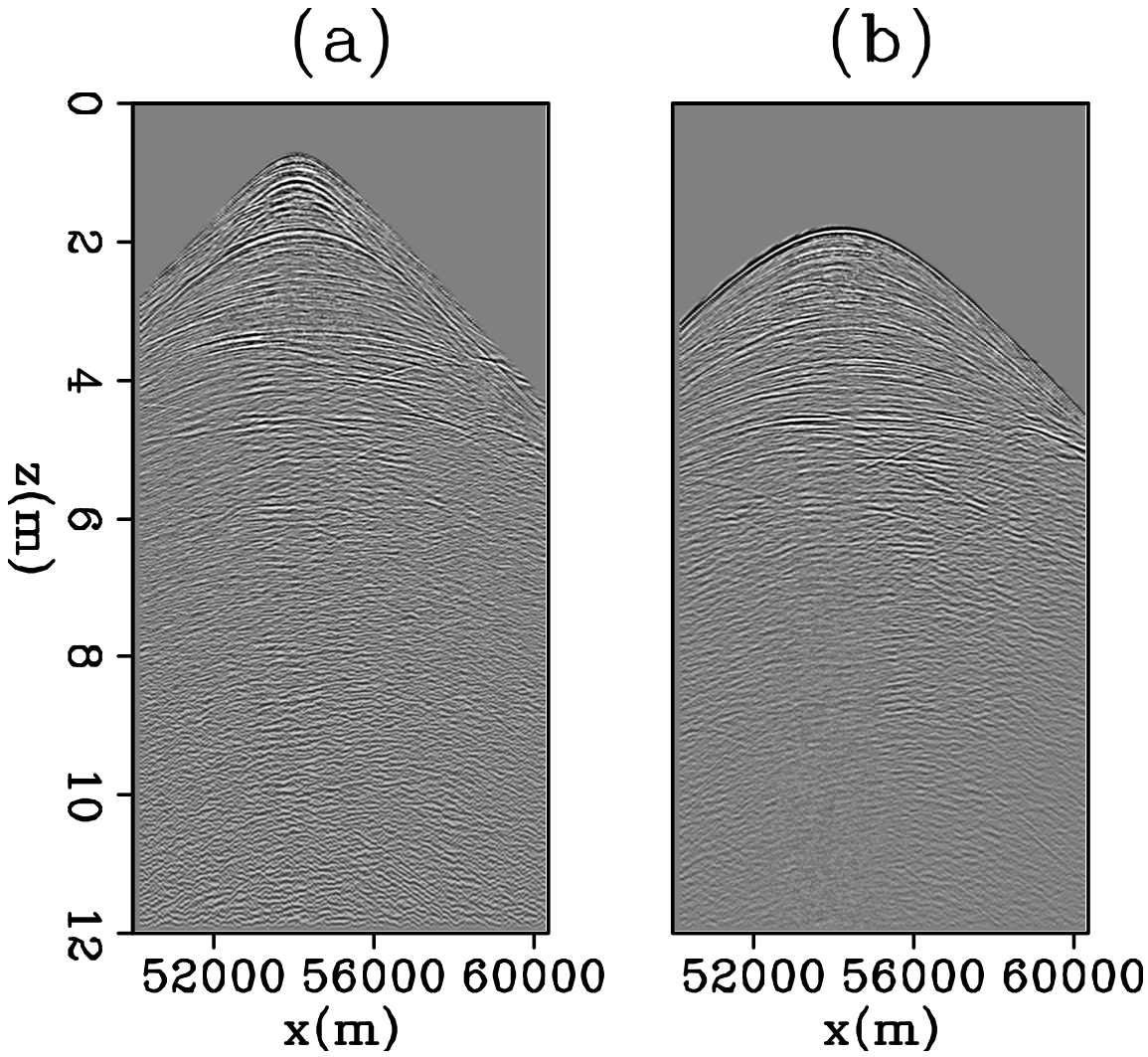

Figure 10: One common receiver gather of the (a) up-going primary and (b) down-going mirror data. [**CR**]

The conventional imaging scheme for ocean bottom node datasets migrate only the down-going mirror (Ronen et al., 2005; Dash et al., 2009) signal. Often time, more care is given to the down-going mirror signal than the up-going signal. We observe that the down-going data is better separated than the up-going data. Figure 11a shows the imaging result when we apply the down-going migration operator onto the up-going data. We can represent this mathematically with:

$$\mathbf{m}_{xalk} = \mathbf{L}_{\downarrow}^{T}\mathbf{d}_{\uparrow}. \tag{12}$$

Figure 11b shows the image from applying the down-going migration operator onto the down-going data. We can identify some of the events that are presence in either of the two images. For example the reflectors annotated in Figure reffig:xtalkdeimos can be found in both images. This suggests that some residual down-going energy remains in the up-going data.

When unaccounted energy is present in the field dataset, it compromises both the RTM and the LSRTM results. In the LSRTM case, the inversion will adjust the solution to try to explain some of the crosstalk energy in the data. To alleviate this problem, I have applied the extended domain noise filtering scheme to remove some of the unwanted energy in the image space.

Imaging with a single mode

In conventional imaging, the down-going mirror signal is used for migration because it provides a wider illumination area. Often time, the up-going signal is not used in imaging. This is because the illumination area of the primary reflection is often much narrower than that from the mirror reflection. Figure 12 shows the relative illumination area (highlighted in yellow) of the primary and mirror events. The mirror signal can clearly illuminate the sea-bottom region much better than the primary signal.

Figure 13 shows the RTM image using the primary signal and the mirror-only signal. Notice that the illumination area between Figure 13a and b is not as dramatically different as described by Figure 12. This is because the lateral extend of the source grid is only slightly larger than the lateral extend of the receiver grid along the inline direction. Although the illumination between the up-going and down-going signals are similar for this survey, joint-imaging could still be beneficial in terms of higher signal to noise ratio for the image. I will show you some of the joint imaging results in the next section.

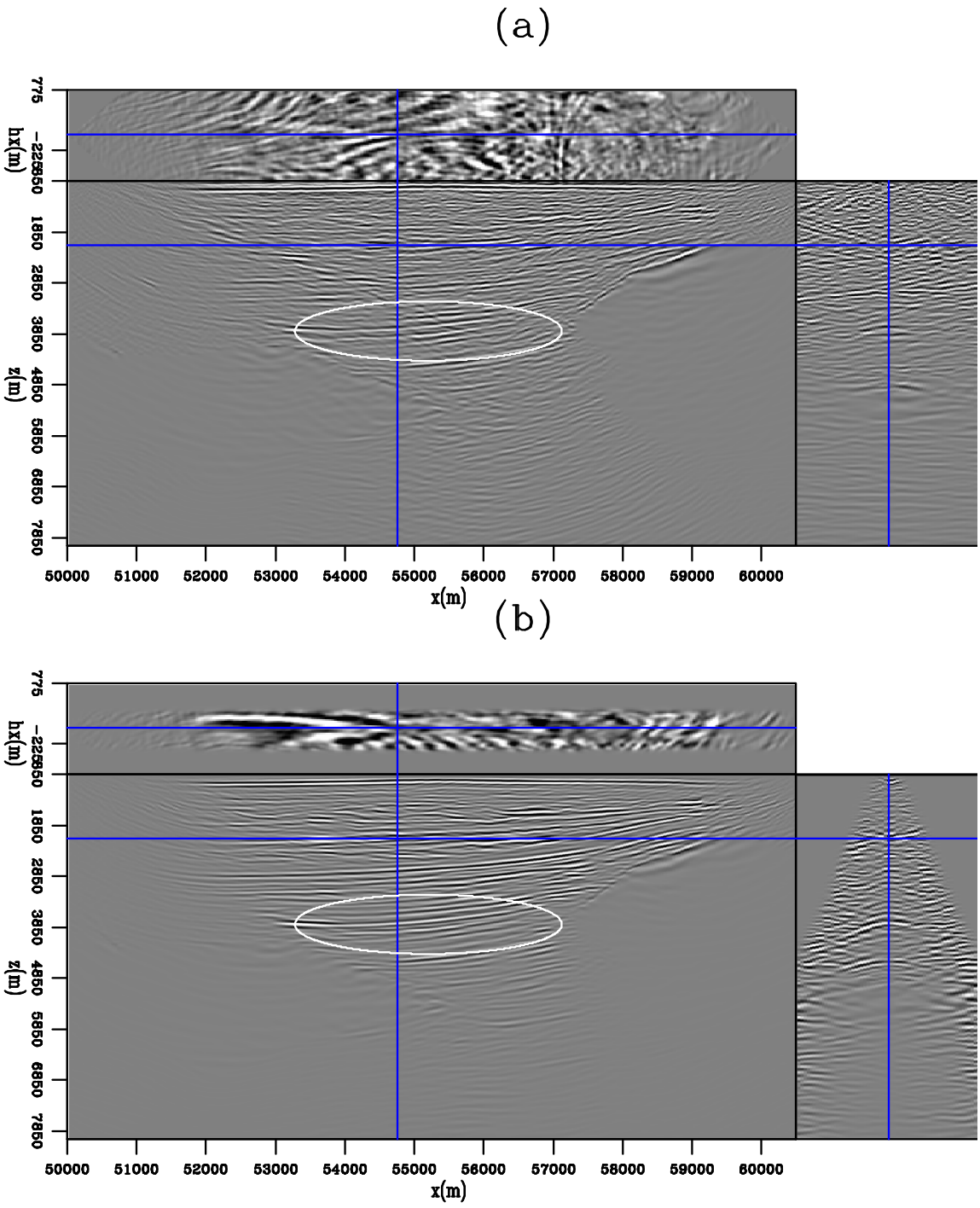

Figure 11: Image depicting crosstalk energy when applying the down-going migration operator onto the up-going data; $\mathbf{m}_{xalk} = \mathbf{L}_{\downarrow}^{T}\mathbf{d}_{\uparrow}$. [**CR**]

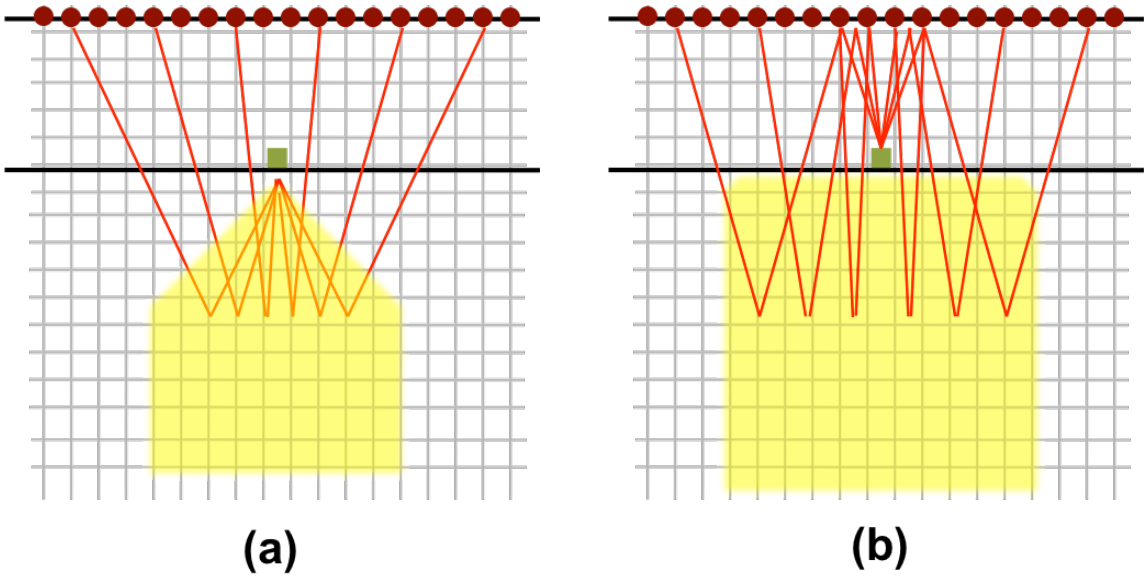

Figure 12: The relative illumination area (highlighted in yellow) of the (a) primary and (b) mirror events for ocean bottom node geometry. [**NR**]

Joint imaging of up- and down-going ocean bottom signals with LSRTM

Figure 14a shows the joint-RTM image and Figure 14b shows the joint-LSRTM image. The joint-RTM image is essentially the first gradient of the joint-LSRTM algorithm. It can also be viewed as the sum of the up-going RTM image and the down-going RTM image. As compared to conventional mirror image (Figure 13b) and the joint-RTM image (Figure 14a), the joint-LSRTM image has better relative amplitude balance for the deeper reflectors.

One challenging area to image in the Deimos field is up against the Antares salt. Burch et al. (2010) proposed using 3D VSP survey to improve illumination in that region (Figure 15). We will look at how joint-LSRTM performs in a nearby region as depicted by Figure 15.

Figure 16 shows an enlarged section near the Antares salt for the down-going RTM and down-going LSRTM images. Figure 17 shows the corresponding enlarged sections of the joint-RTM and joint-LSRTM images. Comparing the two figures, we can see that the joint-LSRTM has improved illumination near the salt flank. The side-panel in Figure 17b shows that the energy is more focused at zero-subsurface offset for reflectors close to the salt flank.

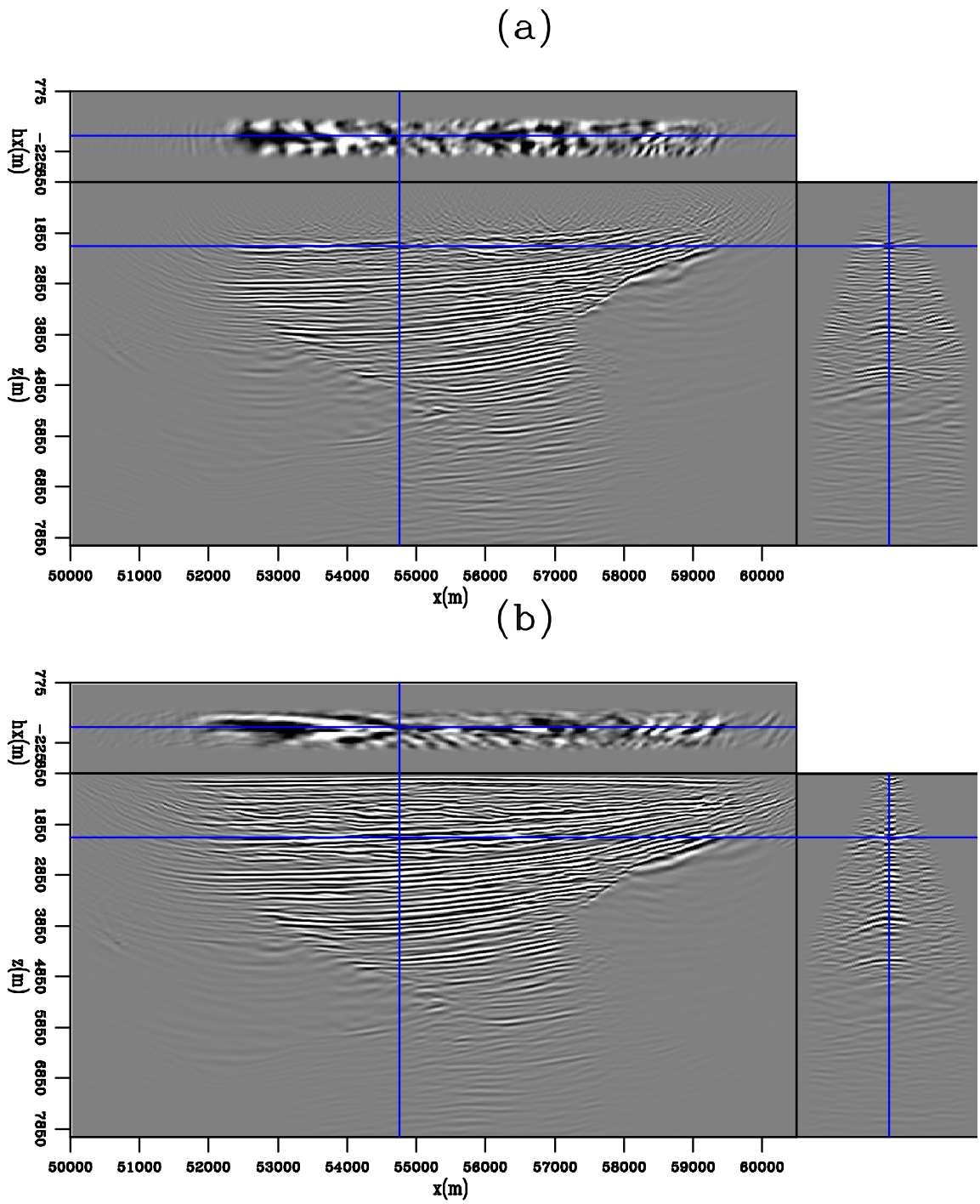

Figure 13: Subsurface offset RTM image gather using (a) the up-going primary signal and (b) the down-going mirror signal. The front face shows the image gather at zero-subsurface offset. [**CR**]

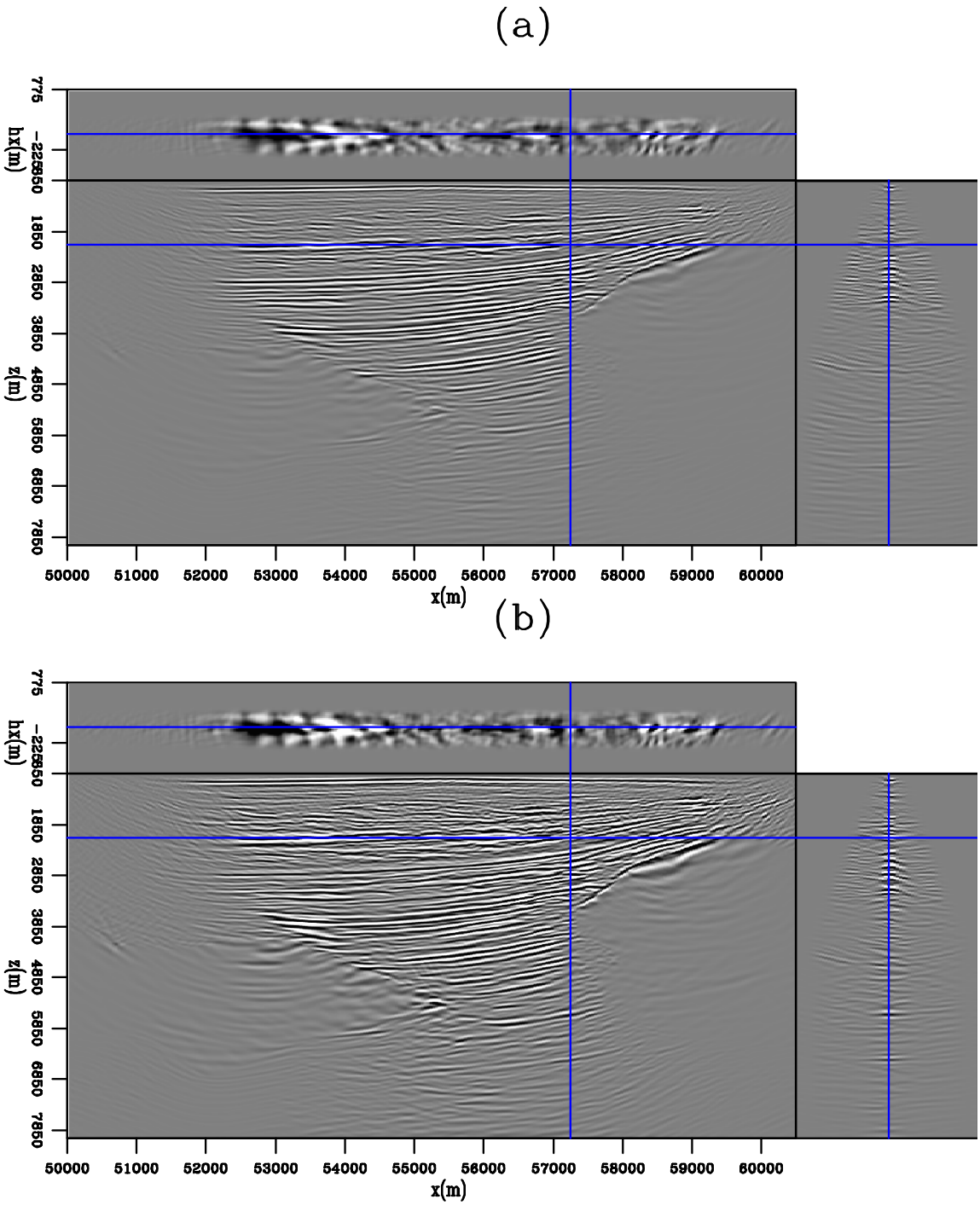

Figure 14: (a) joint-RTM image. (b) joint-LSRTM image at iteration 25. [**CR**]

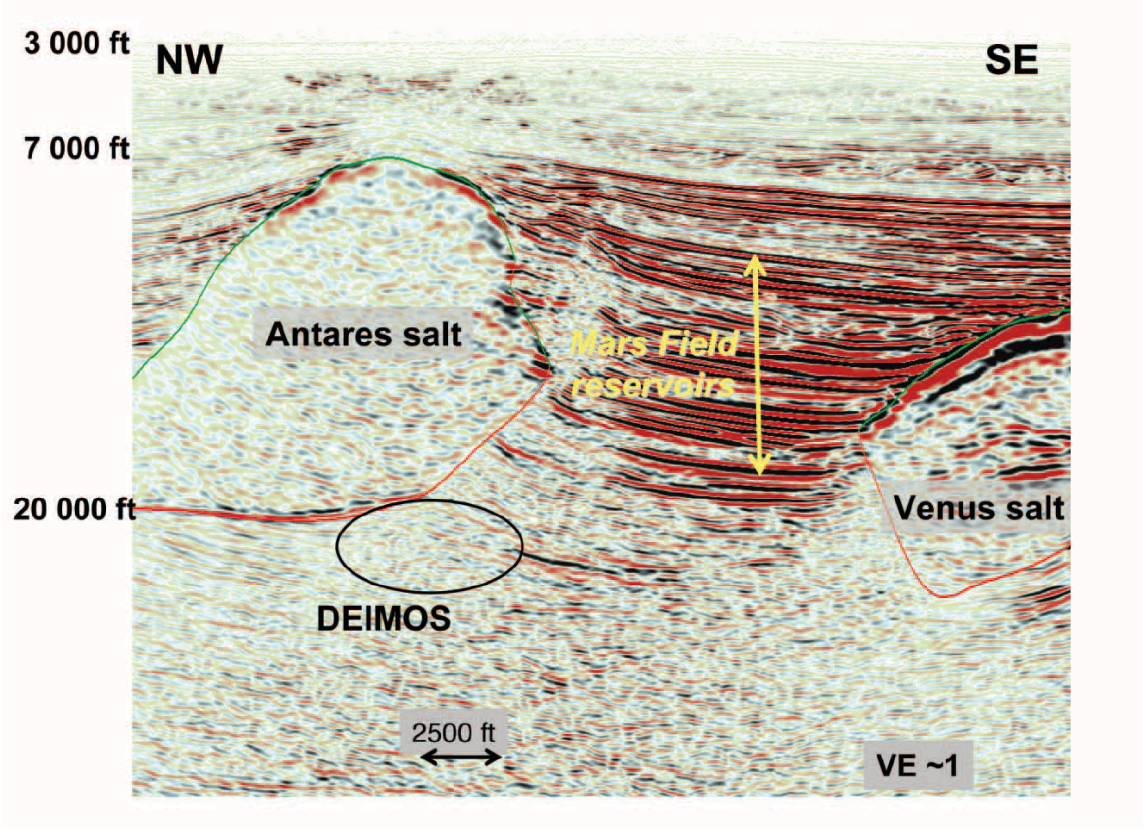

Figure 15: A migration image of the 2007 survey with 807 ocean bottom nodes. The Deimos field is indicated by the oval below the Antares salt. This figure is from Burch et al. (2010). [**NR**]

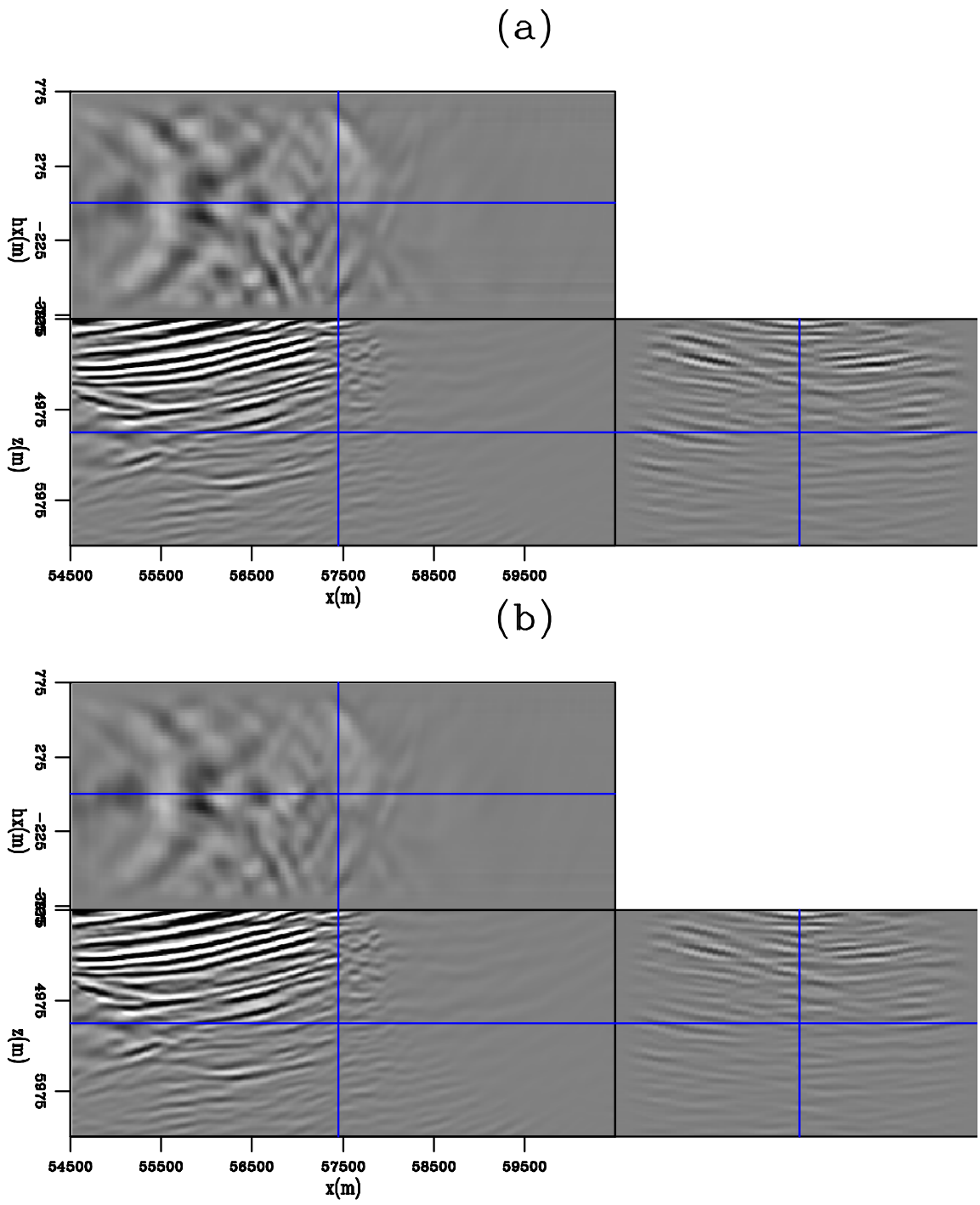

Figure 16: A enlarged section near the Antares salt for (a) the down-going RTM image and (b) the down-going LSRTM image at iteration 25. [**CR**]

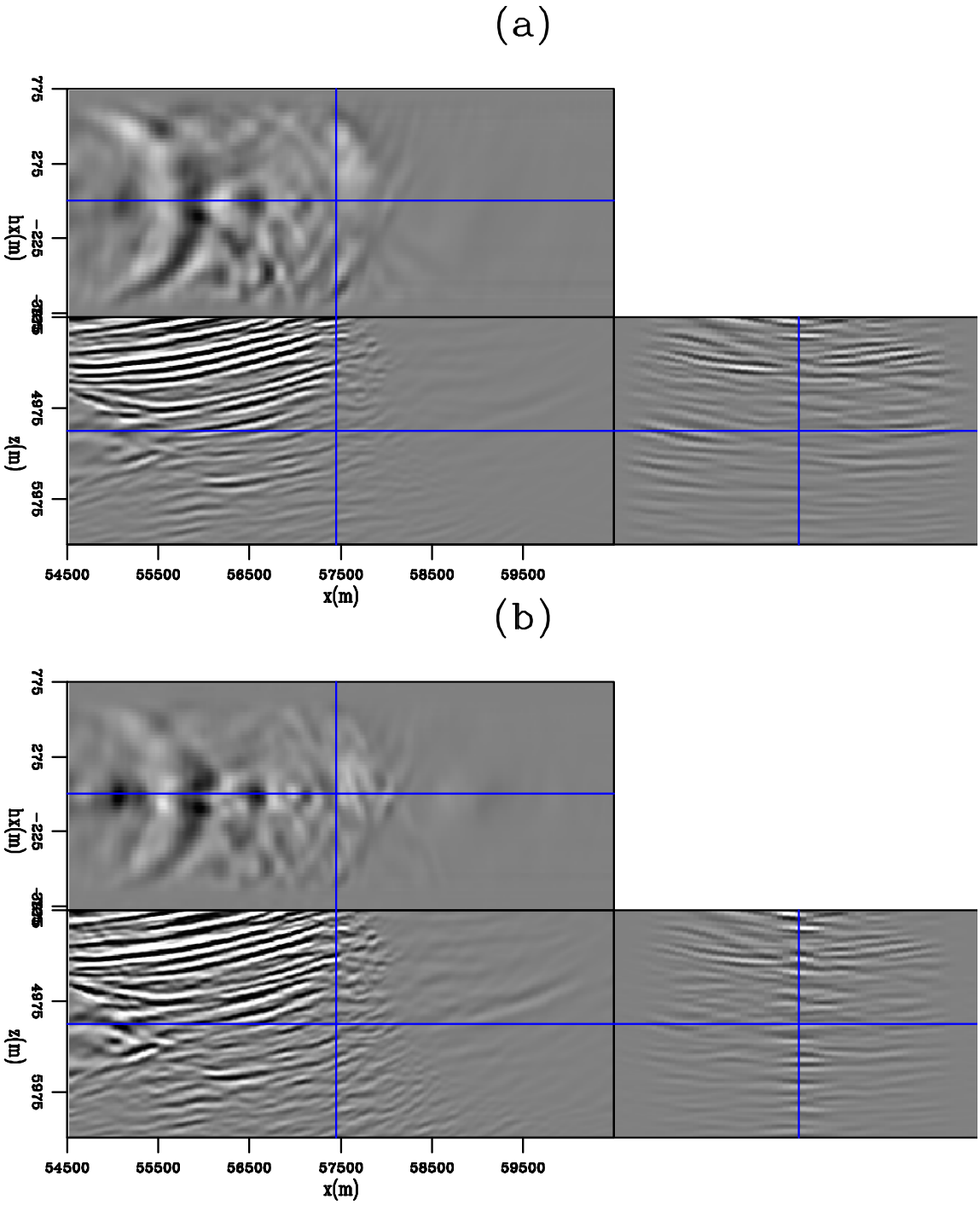

Figure 17: A enlarged section near the Antares salt for (a) the joint-RTM image and (b) the joint-LSRTM image at iteration 25. Notice that the reflectors against the salt flank near the Deimos field are better illuminated. The side-panel in (b) shows that the energy is more focused at zero-subsurface offset. [**CR**]

DISCUSSION

The result from Figure 17 is encouraging. However, more investigation is needed to study the contribution from the up-going and the down-going signal onto the joint-image. There are several future directions that we would like to pursue. Oneis to apply target oriented data space weighting to enphasize the subsalt region. Another direction is to use iterative reweighted least-squares for the inversion.

CONCLUSION

Least-squares reverse time migration is an advanced imaging technique that can improve imaging with better relative amplitude information, fewer artifacts, and reduced noise. When applying to field data sets, the recorded data departs from the theory and assumptions of the LSRTM operator. It is found that a simple data-fitting objective function in LSRTM is not sufficient. We used Laplacian preconditioning, salt-dimming data weighting, noise filtering in the extended domain, and DSO regularization to condition the LSRTM algorithm when applied to the 3D Deimos ocean bottom field data set. By comparing the joint-LSRTM image of up- and down-going signal with the conventional down-going RTM or down-going LSRTM images, we see better relative amplitude balance for the reflectors and improved illumination near the Antares salt area.

ACKNOWLEDGMENTS

The authors wish to thank Shell Exploration and Production Company, as well as BP Americas for permission to publish this work. Mandy thanks Michael Merritt, Richard Cook, Colin Perkins, Vanessa Goh, and Alexander Stopin for their data processing, helpful suggestions and discussions.

REFERENCES

Burch, T., B. Hornby, H. Sugianto, and B. Nolte, 2010, Subsalt 3d vsp imaging at deimos field in the deepwater gulf of mexico: The Leading Edge, **29**, 680–685.

Clapp, M. L., 2005, Imaging under salt: illumination compensation by regularized inversion: PhD thesis, Stanford University.

Dash, R., G. Spence, R. Hyndman, S. Grion, Y. Wang, and S. Ronen, 2009, Wide-area imaging from obs multiples: Geophysics, **74**, Q41–Q47.

Hays, D., K. Craft, P. Docherty, and F. Smit, 2008, An ocean bottom seismic node repeatability study: SEG Technical Program Expanded Abstracts, 55–59.

Lambare, G., J. Virieux, R. Madariaga, and S. Jin, 1992, Iterative asymptotic inversion in the acoustic approximation: Geophysics, **57**, 1138–1154.

Nemeth, T., C. Wu, and G. T. Schuster, 1999, Least-squares migration of incomplete reflection data: Geophysics, **64**, 208–221.

Ronen, S., L. Comeaux, and J. Miao, 2005, Imaging downgoing waves from ocean bottom stations: 75th SEG Annual Meeting Expanded Abstracts, 963–966.

Ronen, S. and C. Liner, 2000, Least-squares dmo and migration: Geophysics, 1364–1371.

Smit, F., C. Perkins, L. Lepre, K. Craft, and R. Woodard, 2008, Seismic data acquisition using ocean bottom seismic nodes at the deimos field, gulf of mexico: SEG Technical Program Expanded Abstracts, 998–1002.

Stopin, A., M. M. Rae, L. Lepre, and B. Gaudin, 2008, Constructing an anisotropic velocity model for ocean bottom seismic node data: SEG Technical Program Expanded Abstracts, 993–997.

Valenciano, A., 2008a, Imaging by Wave-Equation Inversion: PhD thesis, Stanford University.

Valenciano, A. A., 2008b, Imaging by wave-equation inversion: PhD thesis, Stanford University.

Wong, M., 2013, Handling salt reflection in least-squares rtm: SEG Expanded Abstracts, 3921–3925.

Wong, M., B. Biondi, and S. Ronen, 2010, Joint least-squares inversion of up- and down-going signal for ocean bottom data sets: SEG Expanded Abstracts, 2752–2756.

Zhang, Y. and J. Sun, 2009, Practical issues in reverse time migration: true amplitude gathers, noise removal and harmonic source encoding: First Break, **27**, 53–59.